Deep-UV fluorescence lifetime imaging microscopy

Christiaan J. de Jong,[1,2,†] Alireza Lajevardipour,[1,†] Mindaugas Gecevičius,[3,†] Martynas Beresna,[3,†] Gediminas Gervinskas,[1,4,†] Peter G. Kazansky,[3,†] Yves Bellouard,[5,†] Andrew H. A. Clayton,[1,†] and Saulius Juodkazis[1,4,6,*,†]

[1]*Centre for Micro-Photonics, Faculty of Science, Engineering and Technology, Swinburne University of Technology, Hawthorn, VIC 3122, Australia*
[2]*Department of Mechanical Engineering, Eindhoven University of Technology, Postbus 513, 5600MB Eindhoven, The Netherlands*
[3]*Optoelectronics Research Centre, University of Southampton, Southampton, SO17 1BJ, UK*
[4]*Melbourne Centre for Nanofabrication, 151 Wellington Road, Clayton, VIC 3168, Australia*
[5]*Ecole Polytechnique Fédérale de Lausanne, Rue de la Maladiére 71b, CH—2002 Neuchâtel, Switzerland*
[6]*Center for Nanotechnology, King Abdulaziz University, Jeddah 21589, Saudi Arabia*
**Corresponding author: sjuodkazis@swin.edu.au*

Received July 2, 2015; revised August 21, 2015; accepted August 22, 2015; posted August 24, 2015 (Doc. ID 244203); published September 28, 2015

A novel fluorescence lifetime imaging microscopy (FLIM) working with deep UV 240–280 nm wavelength excitations has been developed. UV-FLIM is used for measurement of defect-related fluorescence and its changes upon annealing from femtosecond laser-induced modifications in fused silica. This FLIM technique can be used with microfluidic and biosamples to characterize temporal characteristics of fluorescence upon UV excitation, a capability easily added to a standard microscope-based FLIM. UV-FLIM was tested to show annealing of the defects induced by silica structuring with ultrashort laser pulses. Frequency-domain fluorescence measurements were converted into the time domain to extract long fluorescence lifetimes from defects in silica.

OCIS codes: (110.0180) Microscopy; (260.7190) Ultraviolet; (350.3390) Laser materials processing.
http://dx.doi.org/10.1364/PRJ.3.000283

1. INTRODUCTION

Femtosecond laser direct writing is a powerful technique with applications ranging from optofluidics and optomechanics [1–3] to birefringent optical elements [4] and optical data storage [5]. Under certain experimental conditions, femtosecond laser irradiation can induce self-assembled nanostructure in the bulk of transparent material [6–8] or imprint complex polarization fields onto a surface [9–11]. The subwavelength arrangement of this modification results in optical anisotropy (the form birefringence), which provides control over polarization of traversing light; hence, polarization controlling optical elements can be made using nanogratings. The nanogratings are observed only in a handful of materials such as sapphire, tellurium oxide, germanium oxide, and silica glasses. The mechanisms of nanograting and surface ripple formation are closely related and are actively researched (for a recent review [11]). The bulk ripples are formed at subcritical free carrier plasma densities; the breakdown occurs at the permittivity $\varepsilon' = 0$ (real part) when the critical plasma density is reached. At a higher excitation and over-critical plasma densities when $\varepsilon' \leq -1$ a surface wave (the surface plasmon polariton) can be formed, which is imprinted onto the surface by ablation [11]. In both cases of the bulk and surface ripples, the period is closely following $\Lambda = \lambda_0/n(I)/2$, where the refractive index n is intensity, I, dependent, and λ_0 is the light wavelength in vacuum [11].

Formation of the nanostructure in dielectrics is accompanied by the rearrangement of chemical bonds and formation of optically, magnetically, and electrically active defects. Some of them, under UV irradiation, emit strong fluorescence, which is detectable from the laser-structured areas that can strongly impede imaging and fluorescence lifetime measurements popular in bio and medical research. The fluorescence lifetime imaging microscopy (FLIM) has become a popular technique in cell imaging and is used for investigation of energy transfer mechanisms and can deliver a super-resolution capability [12–14]. Addition of UV functionality to FLIM is an appealing direction due to a possibility of direct excitation of proteins [15] without their labeling. Further insight into germicidal properties of deep-UV (240–280 nm) light [16–18] could be achieved with UV-FLIM. LEDs are used in FLIM, however, not in deep UV range [19].

Here, we show the UV capability, which can be added to standard microscope-based FLIM setups. This UV-FLIM functionality is demonstrated by fluorescence analysis of laser-induced defects in silica where polarization converters were formed by fs-laser writing. It is shown that annealing at 300°C for 2 h fully removes the fluorescence at 650 nm and longer wavelengths without suppressing the form birefringence required for polarization conversion. The UV-fluorescence-lifetime-imaging method revealed the removal of long-time relaxation components from the fluorescence time decay in the defect-fluorescence band in silica. This expands use of fluorescence under UV excitation demonstrated for recognition of protein crystals [20].

2. METHOD

The frequency domain realization of FLIM is based on the temporal modulation of the excitation and on the synchronized detection of the phase-shifted signal [12–14]. To characterize

the temporal properties of fluorescence, the frequency-domain approach was utilized, wherein the lifetime is de termined from the phase, ϕ, and modulation, M, of the fluorescence signal. Typical phasor presentation A versus B is a convenient method to show the phase and modulation values:

$$B = M\ \cos(\phi), \qquad A = M\ \sin(\phi). \tag{1}$$

This method is well suited to measure fluorescence of dye–nanoparticle mixtures in water solutions [21] and is extended to measure the fluorescence from the defects in solid-state materials.

Phase modulation implemented in the FLIM measurements allows much broader time resolution and more detailed information on the fluorescence transients as compared with the standard pump-probe measurements, which usually cannot cover such a vast span of lifetimes. Additionally, UV-FLIM measurements provide information with spatial resolution of 2–3 μm using standard microscopy setup.

The UV-LED-Controller (OptoTech Pty Ltd) tunes the duty cycle of the LED emission from 1 to 1/10 for repetition rates up to 1 MHz. Thanks to this modality, the maximum current can be as high as 20 mA for the light emission duration of the cycle. Deep-UV LEDs at 250–290 nm wavelength (SETi, Inc.) spectral range were used to excite fluorescence from microparticles [22]. UV-LED controller, power supply, and housing are all combined into a compact jig, which can be placed directly onto a microscope objective; the size of a portable jig was 135 mm × 45 mm × 25 mm ($l \times w \times h$).

FLIM data acquisition and analysis were carried out with a commercial setup (LIFA, Lambert Instruments). The signal-to-noise ratio in fluorescence detection was up to 10^3 and allowed us to explore the broad dynamic range of decay times. All data were taken after a high-fidelity (within a confidence range of 0.98) fit of experimental data using the least-squares iterative re-convolution based on the minimization of the weighted sum of the residuals implemented in the Lambert Instruments software. This procedure was carried for multiexponential fits at up to 10 modulation frequencies. Sampling rate and acquisition times were chosen by software to reach the requested high-fidelity fits at each frequency. All multifrequency acquisition took up to a few minutes.

3. RESULTS

In the experiments, the UV-FLIM setup was realized on the basis of a commercial FLIM setup (LIFA, Lambert Instruments), as is shown in Fig. 1. The UV LED excitation source was placed directly onto the microscope sample stage

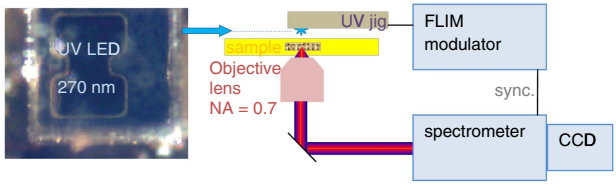

Fig. 1. Realization of UV-FLIM with UV-LED emitting at 270 nm. Custom-designed LED controller (UV-jig) was synchronized with FLIM electronics. Samples used: cells, water-dissolved dyes in microfluidic capillary, laser-structured regions inside silica glass. Footprint of the LED (left) is 2 mm × 2 mm.

for illumination of samples. Leads of a standard TO-18 can housing of the UV-LED were shortened to reduce the RC constant and to achieve high LED switching rates. LED was placed on laser fabricated sample directly without any collimation optics and was used at maximum average power of several microwatts (current of 20 mA).

The FLIM measurements were performed on femtosecond laser written polarization converters (Fig. 2) designed for 532 nm wavelength [4]. The converters have an azimuthally varying pattern of nanogratings, which defines the optical function of the converter. Such converters are the q plates [23], which are inhomogeneous birefringent plates with a topological defect of charge q for the azimuthal pattern of the optical axis. The azimuthal dependence of the slow axis is given by $\Psi = q\varphi$; here, q is the half integer and φ the polar angle. The q plates are used to control the spin-orbital conversion of beams and have an increasing number of applications from microfluidics to quantum computing (see [24]). The polarization converters, q plates, used in this study are made small for integration into a microfluidic channel and realization of (1) an optomechanical momentum transfer element or (2) structured light illumination of microparticles in the channel.

A. Fluorescence From Polarization Converters Illuminated by Deep-UV LEDs

Under illumination of the polarization converter with a 474 nm laser diode at several tens-of-mW power light, a strong red fluorescence could be detected, which can be attributed to the nonbridging oxygen hole center (NBOHC) emission at 650 nm [25], as shown in Fig. 2. Because the form birefringence exhibited by nanogratings is spectrally broadband, the fluorescence at wavelengths longer than $\lambda_l = 560$ nm (a long-pass filter) shows an intensity distribution with a peculiar reminiscence of a phase pattern typical to an optical vortex. This is caused by polarization dependence of the fluorescence excitation and emission due to the presence of the nanogratings. The form-birefringent nanogratings create the same pattern of the defects in silica. The linearly polarized LED

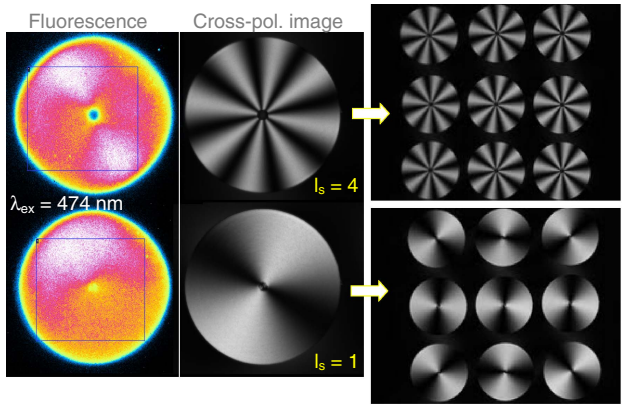

Fig. 2. (Left to right) Fluorescence (false color) image after a long-pass filter $\lambda_l = 560$ nm; the excitation wavelength was $\lambda_{ex} = 474$ nm. Cross-polarized images under white light illumination revealing the polarization converters of the topological charge $l_s = 2q = 4$ (upper) and $l_s = 1$ (lower). Arrays of polarization converters 3 × 3 of different charges and with different orientations were recorded in a silica glass piece that forms the base of a microfluidic channel; the converters diameter is 600 μm.

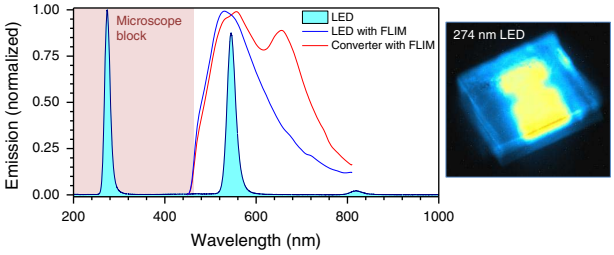

Fig. 3. Emission spectra from the 270 nm LED with peak at 274 nm and its higher-order diffractions at 548 and 822 nm measured without microscope optics, emission of the same LED detected with FLIM microscope, and emission detected from the polarization converter in silica illuminated by the LED. The shaded region marks wavelengths blocked by the microscope optics. Inset shows a false color image (representing intensity) of LED taken with the FLIM setup.

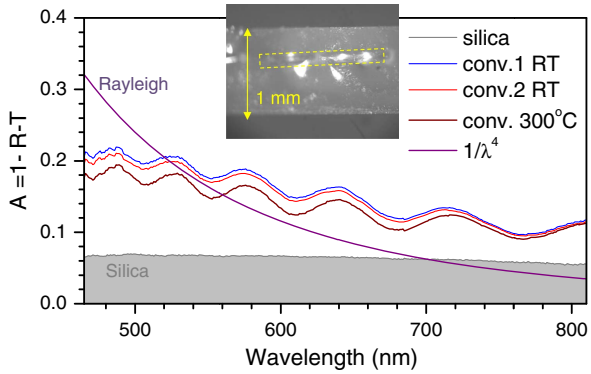

Fig. 4. Absorbance, A, spectra of polarization converters as fabricated (at room temperature RT) and annealed at 300°C for 2 h; transmission $T = 10^{-\mathrm{OD}} = e^{-\alpha d}$, where d is thickness and α (cm^{-1}) is the absorption coefficient. Spectral range is defined by FLIM microscope transmission band. Thickness of glass was $d = 1$ mm and optical thickness of nanogratings (polarization convertor) $d_c \simeq 72$ μm (dashed-box encloser in the inset). The Rayleigh scattering spectral profile is given by λ^{-4}; $R + T + A = 1$ with R accounting for reflection losses.

illumination of such nanogratings creates a fluorescence emission following an angular intensity distribution pattern according to $I_f \propto \cos\theta^2$, where θ is the angle between polarization and the orientation (the wave vector) of the nanogratings. As a result, fluorescence intensity has azimuthal distribution, which might be unwanted in fluorescence measurements. It is noteworthy that the ripple period is affected by the thermal conductivity (temperature diffusivity), which becomes anisotropic along and across the ripples during writing [26]. As a result, thermal accumulation affects the ripple pattern, which is dependent on the writing sequence and proximity of already structured regions. Accordingly, the defect fluorescence becomes dependent on the way to record ripple patterns.

Figure 3 shows the emission spectra of the 270 nm LED measured in air and through the microscope. Free-air emission of the LED has a peak centered at 274 nm, and its second order diffraction is at exactly 548 nm. When the same emission is measured through the FLIM microscope, a broader emission 530 ± 50 nm is observed in the eyepiece of the microscope and spectrometer. In this case, due to filtering of UV components by microscope optics, this emission is related mainly to the defects in LED and partially due to microscope optics. A good image of the LED taken with the microscope suggests that fluorescence originated mainly from the LED, which was placed at the focus (see inset). When the polarization converter is illuminated by the 270 nm LED by placing it onto glass above the laser structured regions, a reddish emission band around 670 nm is recognizable. This band is related to nonbridging oxygen hole center Si-O emission (NBOHC; is the dangling bond) [25,27,28]. The fluorescence image, as shown in Fig. 2, can be obtained under few microwatts excitation at this deep-UV radiation due to emission from NBOHC defects.

B. Post-Annealing Optical Characterization of Polarization Converters

After annealing of converters from 100°C to 300°C, their scattering is slightly decreased, and defect-related fluorescence at 650 nm NBOHC band was fully erased (Fig. 4). The optical density (OD) spectrum showed only a slight reduction of the losses within the spectral window of the FLIM microscope. Annealing at 300°C for 1 h is sufficient to erase the defect-related emission in silica [25,27]. The residual losses are attributed to scattering in nanogratings.

Interference fringes (Fig. 4) are the signature of the nanogratings, which have recognizable (an optical side-view imaging was used) thickness of $d_c \simeq 70$ μm. One can obtain comparable value from the two neighboring interference maxima at wavelengths $\lambda_{1,2} = 526, 576$ nm from $\Delta n d = (1/\lambda_1 - 1/\lambda_2)^{-1}$, where $\Delta n \simeq 8.4 \times 10^{-2}$ is the refractive index of silica and $d = 72$ μm is the apparent thickness of the pattern responsible for interference (thickness of polarization converter). This value is larger than usual modulation of refractive index due to nanograting, which is approximately $\Delta n \sim 10^{-3}$. Possibly, the actual extension of the polarization converter is larger than can be judged from the obvious breakdown regions from side observation [28–31].

C. FLIM Measurements From Defects in Silica

From the phase ϕ and modulation M using a phasor plot $A = f(B)$, the fluorescence lifetime τ is determined. By selecting different modulation frequencies in the range of $f = 0.1$–10 MHz, the lifetime as short as ~1 ns can be retrieved. Figure 5(a) shows raw experimental data and sin-fit, which was used to calculate the phase and modulation of the detected emission at a single fixed modulation frequency. For multiexponential decay processes, a single modulation frequency is insufficient to resolve multiple lifetime decays. Consequently, we determined the phase and modulation values at 10 different modulation frequencies. Figure 5(b) displays the phase and modulation values as a function of modulation frequency for the polarization converters. The solid lines are fits to the dispersion equations appropriate for a multiexponential decay model [32].

Fits are summarized in Fig. 6. To aid visualization of the decay processes in time, the fits to the phase-modulation data are presented in the time domain in Fig. 6.

Fluorescence of the defects usually has a complex stretched exponential behavior. From the FLIM data, the time dependence of fluorescence is expressed by multiexponential expression with a characteristic time τ_i and corresponding amplitude a_i as

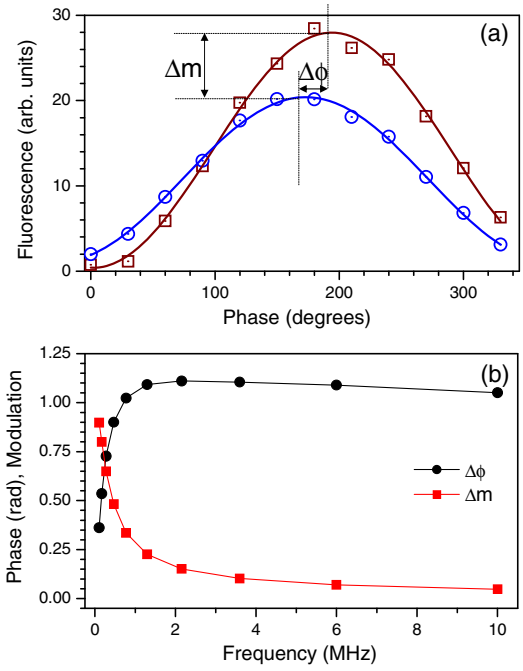

Fig. 5. (a) Phase shifted and modulated FLIM signals from the rhodamine (□) and polarization convertor (○). Phase shift $\Delta\phi$ and change of modulation depth Δm are shown. The best fit to a sin function was used to extract the lifetime τ at a specific 0.1 MHz frequency. Fluorescence intensity error bars <5% were smaller than the marker size. (b) Phase and modulation data from polarization converter. Solid lines represent the best fit to a multiple lifetime model; this representation corresponds to the Fourier transform of the time-domain dependence given by Eq. (2).

$$\text{Fluorescence}(t) = \sum_{i=1}^{n} \frac{a_i}{\tau_i} e^{-\frac{t}{\tau_i}}. \tag{2}$$

We used maximum $n = 5$ for the best fit of the measured FLIM data from the defects in glass. Data are summarized in Fig. 6. Under standard FLIM excitation, $\lambda_{ex} = 474$ nm; thus, the effect of annealing is clearly seen. We observed a slight increase of fluorescence intensity after annealing up to 100°C and a slight change in the decay profile; however, changes were minimal and usually within the uncertainty range of measurements. Such behavior can be explained by defects relaxation [33,34] because fs-laser fabrication is capable to quench metastable states of defects with low activation energy [35].

Annealing up to 300°C was sufficient to strongly decrease fluorescence at times longer than 100 ns consistent with silica defect relaxation time [27]. It was demonstrated earlier that such annealing preserves the form birefringence of laser structure regions because the nanogratings remain intact [36]. A temperature of 300°C corresponds to the activation energy of $E_a = 0.78$ eV.

Under a 270 nm UV LED excitation, the optics of FLIM microscope was acting as a filter (Fig. 3) with very fast decay times [Fig. 6(b)]. Because UV FLIM has never been used before, we tested it on Rhodamine 6G and obtained results close to the single exponential decay of $\tau \simeq 3.97$ ns as for the reference solution from Lambert Instruments. This expected value shows that UV-FLIM can be used with standard dyes. The fluorescence was filtered in two different spectral bands for which different transients were observed. Because under 274 nm excitation wavelength, a wider spectrum of defects is expected to be excited, such filter gating of emission bands provides a tool to characterize the defects induced by fs-laser fabrication. Stretched exponential time decay of the defect-related luminescence is standard in solid-state materials, especially in glasses where electron-hole separation and trap energy positions vary.

4. DISCUSSION

It is expected that UV-FLIM combination with Raman scattering spectroscopy will provide deeper insight into defect and morphological modifications occurring within and around the fs-laser structured volumes. This is key for fabrication of micro-optical elements and waveguides where local mass density and defects are critically important for the designed function and longevity [37–39]. Better understanding of fs-laser structuring is still strongly required, as it can deliver unique new materials [40–42].

An advantage of the frequency-domain-deep UV-LED FLIM system is its considerably lower cost than multiphoton pulsed laser systems or continuum fiber lasers. Frequencies can be tuned to match longer-lived luminescence transients, which would be not practical to measure using time-domain methods due to the required long delay lines.

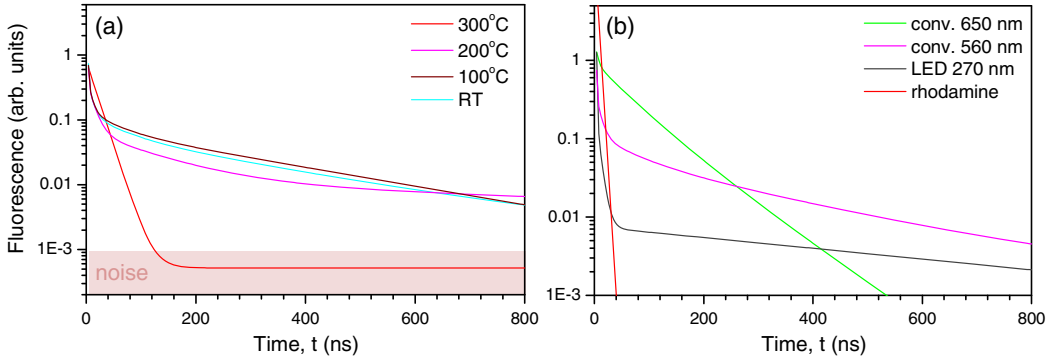

Fig. 6. Multifrequency multiexponential fit of frequency domain FLIM (Fig. 5) using Eq. (2). (a) Fluorescence transients of polarization converter $l_s = 2$ annealed at different temperatures. Excitation wavelength is $\lambda_{ex} = 474$ nm. (b) Fluorescence time decay under $\lambda_{ex} = 270$ nm excitation. Rhodamine 6G showed a $\tau \simeq 4$ ns decay. Polarization converter fluorescence was filtered by bandpass (650 ± 20 nm) and long-pass (560 nm) filters. The direct emission from LED 270 nm measured by FLIM is also presented.

5. CONCLUSIONS AND OUTLOOK

UV-FLIM setup based on a commercial FLIM microscope is demonstrated and extends excitation wavelengths to the shortest 240 nm wavelength available among the state-of-the-art UV LEDs. The spectral bandwidth of the detection path was defined by the microscope; synchronization of UV-LED with FLIM setup was realized by a custom-built controller, which is small enough to place the illumination directly onto a sample mounted on a microscope stage. By controlling the duty cycle of UV illumination, the dedicated electronics allows pulsing operation of the UV-LED with pulse duration down to 20 ns. This setup can be integrated to illuminate microfluidics channels in UV-transparent silica chips or tubes.

Potential use of UV-FLIM for defect characterization in fs-laser structured materials is demonstrated, thus revealing stretched exponential temporal transients. This technique is also promising in biomedical research because it delivers the capability to use FLIM in the frequency domain with light sources, which directly excite proteins by absorption at $\lambda_{ex} < 280$ nm. Because UV-LEDs are widely used in water disinfection, a FLIM capability can provide further information on the effectiveness of the delivered UV dose in incapacitating bacterial, microbial, and viral agents. The UV-FLIM capability can be combined with an imaging mode for samples with spatially variant fluorescence lifetime features.

ACKNOWLEDGMENT

We acknowledge M. Petre and E. Wellner from OptoTech Pty who built electronics for a UV-LED controller and synchronized the controller with a microscope setup. S. J. is grateful for support via the Australian Research Council Discovery DP130101205 and DP120102980 grants and project with Altechna Ltd. We are grateful to E. Brasselet for discussions of q plates and optical vortices. We thank G. Seniutinas and R. Buividas for the technical assistance. C. J. d. J. and A. J. carried out experiments and primary data analysis. M. G. and M. B. fabricated optical vortex generators. GG made first proof-of-the-concept experiments on instrumental capability of deep-UV excited fluorescence. C. J. d. J. and A. H. A. C. worked out methodology of experiments and carried out detailed data analysis. P. G. K. and Y. B. analyzed and discussed the data. A. H. A. C. and S. J. conceived the UV-FLIM idea.

†All the authors contributed to drafting and editing the manuscript.

REFERENCES

1. Y. Bellouard, A. Said, M. Dugan, and P. Bado, "Monolithic three-dimensional integration of micro-fluidic channels and optical waveguides in fused silica," in *Materials Research Society Symposium Proceedings* (Materials Research Society, 1999; 2004), Vol. **782**, pp. 63–68.
2. A. Schaap, Y. Bellouard, and T. Rohrlack, "Optofluidic lab-on-a-chip for rapid algae population screening," Biomed. Opt. Express **2**, 658–664 (2011).
3. Y. Bellouard, A. Said, and P. Bado, "Integrating optics and micromechanics in a single substrate: a step toward monolithic integration in fused silica," Opt. Express **13**, 6635–6644 (2005).
4. M. Beresna, M. Gecevicius, P. G. Kazansky, and T. Gertus, "Radially polarized optical vortex converter created by femtosecond laser nanostructuring of glass," Appl. Phys. Lett. **98**, 201101 (2011).
5. K. Yamasaki, S. Juodkazis, M. Watanabe, H.-B. Sun, S. Matsuo, and H. Misawa, "Recording by micro-explosion and two-photon reading of three-dimensional optical memory in polymethylmethacrylate films," Appl. Phys. Lett. **76**, 1000–1002 (2000).
6. Y. Shimotsuma, P. Kazansky, J. Qiu, and K. Hirao, "Self-organized nanogratings in glass irradiated by ultrashort light pulses," Phys. Rev. Lett. **91**, 247405 (2003).
7. V. Bhardwaj, E. Simova, P. Rajeev, C. Hnatovsky, R. Taylor, D. Rayner, and P. Corkum, "Optically produced arrays of planar nanostructures inside fused silica," Phys. Rev. Lett. **96**, 57404 (2006).
8. F. A. Umran, Y. Liao, M. M. Elias, K. Sugioka, R. Stoian, G. Cheng, and Y. Cheng, "Formation of nanogratings in a transparent material with tunable ionization property by femtosecond laser irradiation," Opt. Express **21**, 15259–15267 (2013).
9. E. G. Gamaly and A. V. Rode, "Physics of ultra-short laser interaction with matter: From phonon excitation to ultimate transformations," Prog. Quantum Electron. **37**, 215–323 (2013).
10. C. Hnatovsky, V. Shvedov, W. Krolikowski, and A. Rode, "Revealing local field structure of focused ultrashort pulses," Phys. Rev. Lett. **106**, 123901 (2011).
11. R. Buividas, M. Mikutis, and S. Juodkazis, "Surface and bulk structuring of materials by ripples with long and short laser pulses: recent advances," Prog. Quantum Electron. **38**, 119–156 (2014).
12. K. P. Ghiggino, M. R. Harris, and P. G. Spizzirri, "Fluorescence lifetime measurements using a novel fiber-optic laser scanning confocal microscope," Rev. Sci. Instrum. **63**, 2999–3003 (1992).
13. A. Clayton, F. Walker, S. Orchard, C. Henderson, D. Fuchs, J. Rothacker, E. Nice, and A. Burgess, "Ligand-induced dimer-tetramer transition during the activation of the cell surface epidermal growth factor receptor-A multidimensional microscopy analysis," J. Biol. Chem. **280**, 30392–30399 (2005).
14. V. R. Caiolfa, M. Zamai, G. Malengo, A. Andolfo, C. D. Madsen, J. Sutin, M. A. Digman, E. Gratton, F. Blasi, and N. Sidenius, "Monomer dimer dynamics and distribution of GPI-anchored uPAR are determined by cell surface protein assemblies," J. Cell Biol. **179**, 1067–1082 (2007).
15. P. Vita, N. Kurilčik, S. Juršėnas, A. Žukauskas, A. Lunev, Y. Bilenko, J. Zhang, X. Hu, J. Deng, T. Katona, and R. Gaska, "Deep-ultraviolet light-emitting diodes for frequency domain measurements of fluorescence lifetime in basic biofluorophores," Appl. Phys. Lett. **87**, 084106 (2005).
16. K. Y. Nelson, D. W. McMartin, C. K. Yost, K. J. Runtz, and T. Ono, "Point-of-use water disinfection using uv light-emitting diodes to reduce bacterial contamination," Environ. Sci. Pollut. Res. **20**, 5441–5448 (2013).
17. M. Shatalov, A. Lunev, X. Hu, O. Bilenko, I. Gaska, W. Sun, J. Yang, A. Dobrinsky, Y. Bilenko, R. Gaska, and M. Shur, "Performance and applications of deep uv led," Int. J. High Speed Electron. Syst. **21**, 1250011 (2012).
18. M. Würtele, T. Kolbe, M. Lipsz, A. Külberg, M. Weyers, M. Kneissl, and M. Jekel, "Application of gan-based ultraviolet-c light emitting diodes-uv leds-for water disinfection," Water Res. **45**, 1481–1489 (2011).
19. J. T. Wessels, U. Pliquett, and F. S. Wouters, "Light-emitting diodes in modern microscopy—from David to Goliath," Cytometry Part A **81A**, 188–197 (2012).
20. R. A. Judge, K. Swift, and C. González, "An ultraviolet fluorescence-based method for identifying and distinguishing protein crystals," Acta Crystallogr. Sect. D **D61**, 60–66 (2005).
21. R. Kubiliūtė, K. Maximova, A. Lajevardipour, J. Yong, J. S. Hartley, A. S. M. Mohsin, P. Blandin, J. W. M. Chon, A. H. A. Clayton, M. Sentis, P. R. Stoddart, A. Kabashin, R. Rotomskis, and S. Juodkazis, "Ultra-pure, water-dispersed au nanoparticles produced by femtosecond laser ablation and fragmentation," Int. J. Nanomed. **8**, 2601–2611 (2013).
22. G. Gervinskas, P. R. Stoddart, A. H. A. Clayton, A. Žukauskas, and S. Juodkazis, "Light extraction and fluorescence in UV micro-fluidic applications," Proc. AIP **21**, 29 (2012).
23. L. Marrucci, C. Manzo, and D. Paparo, "Optical spin-to-orbital angular momentum conversion in inhomogeneous anisotropic media," Phys. Rev. Lett. **96**, 163905 (2006).
24. L. Marrucci, E. Karimi, S. Slussarenko, B. Piccirillo, E. Santamsato, E. Nagali, and F. Sciarrino, "Spin-to-orbital conversion of the angular momentum of light and its classical and quantum applications," J. Opt. **13**, 064001 (2011).

25. M. Watanabe, S. Juodkazis, H.-B. Sun, S. Matsuo, and H. Misawa, "Luminescence and defect formation by visible and near-infrared irradiation of vitreous silica," Phys. Rev. B **60**, 9959–9964 (1999).
26. R. Buividas, S. Rekštytė, M. Malinauskas, and S. Juodkazis, "Nano-groove and 3D fabrication by controlled avalanche using femtosecond laser pulses," Opt. Mater. Express **3**, 1674–1686 (2013).
27. H.-B. Sun, S. Juodkazis, M. Watanabe, S. Matsuo, H. Misawa, and J. Nishii, "Generation and recombination of defects in vitreous silica induced by irradiation with near-infrared femtosecond laser," J. Phys. Chem. **104**, 3450–3455 (2000).
28. O. Efimov, S. Juodkazis, and H. Misawa, "Intrinsic single and multiple pulse laser-induced damage in silicate glasses in the femtosecond-to-nanosecond region," Phys. Rev. A **69**, 042903 (2004).
29. S. Juodkazis, S. Matsuo, H. Misawa, V. Mizeikis, A. Marcinkevicius, H. B. Sun, Y. Tokuda, M. Takahashi, T. Yoko, and J. Nishii, "Application of femtosecond laser pulses for microfabrication of transparent media," Appl. Surf. Sci. **197–198**, 705–709 (2002).
30. S. Juodkazis, K. Yamasaki, V. Mizeikis, S. Matsuo, and H. Misawa, "Formation of embedded patterns in glasses using femtosecond irradiation," Appl. Phys. A **79**, 1549–1553 (2004).
31. E. Vanagas, I. Kudryashov, D. Tuzhilin, S. Juodkazis, S. Matsuo, and H. Misawa, "Surface nanostructuring of borosilicate glass by femtosecond nJ energy pulses," Appl. Phys. Lett. **82**, 2901–2903 (2003).
32. E. Gratton, D. M. Jameson, and R. D. Hall, "Multifrequency phase and modulation fluorometry," Annu. Rev. Biophys. Bioeng. **13**, 105–124 (1984).
33. S. Juodkazis, P. Eliseev, H.-B. Sun, M. Watanabe, H. Misawa, T. Sugahara, and S. Sakai, "Annealing of GaN-InGaN multi quantum wells: correlation between the bangap and yellow photoluminescence," Jpn. J. Appl. Phys. **39**, 393–396 (2000).
34. P. Eliseev, H.-B. Sun, S. Juodkazis, T. Sugahara, S. Sakai, and H. Misawa, "Laser-induced damage threshold and surface processing of GaN at 400 nm wavelength," Jpn. J. Appl. Phys. **38**, L839–L841 (1999).
35. T. Hashimoto, S. Juodkazis, and H. Misawa, "Void formation in glass," New J. Phys. **9**, 253 (2007).
36. M. Beresna, M. Gecevičius, M. Lancry, B. Poumellec, and P. G. Kazansky, "Broadband anisotropy of femtosecond laser induced nanogratings in fused silica," Appl. Phys. Lett. **103**, 131903 (2013).
37. S. Juodkazis, V. Mizeikis, M. Sudžius, H. Misawa, K. Kitamura, S. Takekawa, E. G. Gamaly, W. Z. Krolikowski, and A. V. Rode, "Laser induced memory bits in photorefractive $LiNbO_3$ and $LiTaO_3$," Appl. Phys. A **93**, 129–133 (2008).
38. S. Juodkazis, H. Misawa, T. Hashimoto, E. Gamaly, and B. Luther-Davies, "Laser-induced micro-explosion confined in a bulk of silica: formation of nano-void," Appl. Phys. Lett. **88**, 201909 (2006).
39. L. Bressel, D. de Ligny, C. Sonneville, V. Martinez-Andrieux, V. Mizeikis, R. Buividas, and S. Juodkazis, "Femtosecond laser induced density changes in GeO_2 and SiO_2 glasses: fictive temperature effect," Opt. Mater. Express **1**, 605–613 (2011).
40. S. Juodkazis, H. Misawa, E. G. Gamaly, B. Luther-Davis, L. Hallo, P. Nicolai, and V. Tikhonchuk, "Is the nano-explosion really microscopic?" J. Non-Cryst. Solids **355**, 1160–1162 (2009).
41. S. Juodkazis, K. Nishimura, S. Tanaka, H. Misawa, E. E. Gamaly, B. Luther-Davies, L. Hallo, P. Nicolai, and V. Tikhonchuk, "Laser-induced microexplosion confined in the bulk of a sapphire crystal: Evidence of multimegabar pressures," Phys. Rev. Lett. **96**, 166101 (2006).
42. E. E. Gamaly, S. Juodkazis, K. Nishimura, H. Misawa, B. Luther-Davies, L. Hallo, P. Nicolai, and V. Tikhonchuk, "Laser-matter interaction in a bulk of a transparent solid: confined microexplosion and void formation," Phys. Rev. B **73**, 214101 (2006).